

A Consensus Algorithm-Based Secondary Control With Low Vulnerability in Microgrids

Xiao, Junjie; Wang, Lu; Bauer, Pavol; Qin, Zian

DOI

[10.1109/TII.2024.3523566](https://doi.org/10.1109/TII.2024.3523566)

Publication date

2025

Document Version

Final published version

Published in

IEEE Transactions on Industrial Informatics

Citation (APA)

Xiao, J., Wang, L., Bauer, P., & Qin, Z. (2025). A Consensus Algorithm-Based Secondary Control With Low Vulnerability in Microgrids. *IEEE Transactions on Industrial Informatics*, 21(4), 3196-3205.
<https://doi.org/10.1109/TII.2024.3523566>

Important note

To cite this publication, please use the final published version (if applicable).
Please check the document version above.

Copyright

Other than for strictly personal use, it is not permitted to download, forward or distribute the text or part of it, without the consent of the author(s) and/or copyright holder(s), unless the work is under an open content license such as Creative Commons.

Takedown policy

Please contact us and provide details if you believe this document breaches copyrights.
We will remove access to the work immediately and investigate your claim.





Green Open Access added to TU Delft Institutional Repository

'You share, we take care!' - Taverne project

<https://www.openaccess.nl/en/you-share-we-take-care>

Otherwise as indicated in the copyright section: the publisher is the copyright holder of this work and the author uses the Dutch legislation to make this work public.

A Consensus Algorithm-Based Secondary Control With Low Vulnerability in Microgrids

Junjie Xiao , Graduate Student Member, IEEE, Lu Wang , Member, IEEE, Pavol Bauer , Senior Member, IEEE, and Zian Qin , Senior Member, IEEE

Abstract—Consensus algorithm-based secondary control, such as virtual impedance, is typically used to achieve power-sharing and ensure stable operation in microgrids. The introduction of communication, however, increases the system's vulnerability. Communication failure, e.g., under cyber attack or disruption, can lead to a huge loss. To solve this, this article proposes a signal reconstruction approach for the miscommunicated signals. The power-sharing convergence, both in normal conditions and under communication failure, is analyzed via the Lyapunov method. The feasibility and effectiveness of the proposed approach are validated on a lab-scale microgrid.

Index Terms—AC microgrid, communication relief, cyber attack, distributed control.

I. INTRODUCTION

MICROGRID technology is a small electrical power system consisting of multiple distributed generator (DG) modules [1]. In medium/high-voltage microgrids, as the feeder features inductive, the Pf and QV droop laws are typically adopted to reach active power sharing [2], [3]. However, the reactive and harmonic power sharing is determined by the feeder impedance [4] and cannot be maintained by the droop control. Improper reactive power sharing can lead to severe circulating currents among the DG units, compromising the stable operation of the microgrid. In addition, harmonic currents generated by nonlinear loads can trigger current protection mechanisms or cause some DG units to overload if they cannot be shared by the involved DGs.

To address this issue, different power-sharing schemes have been developed. A comparison between the proposed method and previous research is shown in Table I. It demonstrates a gradual improvement in control performance, as indicated by the increasing trend of $\circ \bullet \bullet \bullet$, while the symbol \ denotes an inapplicable evaluation index. Intuitively, designing an accurate virtual impedance [5], [6] or properly tuning droop

TABLE I
COMPARED THIS ARTICLE WITH OTHER RESEARCHES

Ref	Line Info	PCC Info	Accuracy	V-quality	Distributed	Com-delay	Com-cost	Com-stop	Resilient
[4]	●	●	○	●	○	●	○	●	○
[5], [6]	●	○	●	○	/	/	/	/	/
[8], [9]	●	●	●	○	/	/	/	/	/
[10], [11]	●	○	●	●	/	/	/	/	/
[13], [14]	●	●	●	●	○	○	○	○	○
[15], [16]	●	●	●	●	●	●	○	○	○
[18]	●	●	●	●	●	●	●	○	○
[20], [21]	●	●	●	●	●	●	●	○	○
[22], [23]	●	●	●	●	●	○	○	●	●
Proposed	●	●	●	●	●	●	●	●	●

coefficient [7] can help contribute to accurate power sharing; however, it is generally impossible to acquire the actual physical line impedance of each feeder in practice. A sizeable virtual impedance is suggested in [8] and [9] to smoothen out the impedance mismatch. However, this may make the bus voltage highly distorted. The methods proposed in [10] and [11] can be utilized to compensate for bus voltage, while it is not easily measured.

As a critical technology for cyber-physical systems [12], communication technology merits adoption to address the power-sharing concerns of microgrids. A centralized microgrid controller (MGCC) is adopted in [13] and [14]. The controller modifies the virtual impedance in real time. However, it relies on the reliability of the centre controller.

To cope with the “single point of failure” in MGCC, the distributed philosophy has been used in the microgrid to enhance its reliability. In [15] and [16], consensus algorithm-based distributed control has recently been implemented in parallel inverter systems. However, this method features a large amount of data exchange among the inverters as it necessitates periodically exchanging data with the neighbor. Unfortunately, the limited communication resources may result in poor performance of the distributed system [17]. Alternatively, a discrete-time communication mechanism is proposed in [18] for relaxing the need for communication to some extent.

The event-triggered control (ETC) framework has drawn increasing interest recently within the multiagent systems

Received 6 August 2024; accepted 16 December 2024. Date of publication 17 January 2025; date of current version 4 April 2025. This work was supported by the China Scholarship Council under Grant 202106280042. Paper no. TII-24-3998. (Corresponding author: Zian Qin.)

The authors are with the DC System, Energy Conversion, and Storage Group, Faculty of Electrical Engineering, Mathematics, and Computer Science, Delft University of Technology, 2628 CD Delft, The Netherlands (e-mail: j.xiao-2@tudelft.nl; l.wang-11@tudelft.nl; p.bauer@tudelft.nl; z.qin-2@tudelft.nl).

Digital Object Identifier 10.1109/TII.2024.3523566

field [19]. Compared to the typical periodic approach, its main advantage is that communication is conducted nonperiodic, and therefore, the communication dependency between individual units can be further reduced. It has been applied in the microgrid filed [20]. Most recently, a dynamic ETC architecture was introduced to reduce communication demands while keeping power sharing. In the hypothesis, the convergence law is only activated when the output power varies [21]. In practice, the huge traffic demands placed on the communication network are not relieved because many loads on the ac bus change frequently.

In addition to the communication dependency issues, the reliance on communication technology of distributed control makes the system vulnerable to cyber-attacks and communication disruption, which can degrade the control accuracy and cause system instability [22], [23]. To cope with the abovementioned issues, we propose, in this article, a resilient communication-based virtual impedance strategy for harmonic and reactive power sharing. With resilience, the secondary control can operate nearly normally, even during attacks. This resilience is achieved through a signal reconstruction mechanism that mitigates the impact of communication failures and reduces the system's vulnerability, and, in the meantime, avoids the converge speed degradation in [22] and [23]. Moreover, it allows the communication to be switched-OFF once the communicated signal is constructed, which reduces the communication dependency in [11], [15], [16], [17], [18], [20], [21], [22], and [23] and vulnerability further.

The rest of this article is organized as follows. Section II discusses the control and power-sharing issues of islanding microgrids. Section III presents the consensus algorithm for reactive power and harmonic power. Section IV discusses the effect of communication failure, resilient control, and communication dependency relief strategy. Section V shows the experimental evaluation of the suggested control method. Finally, Section VI concludes this article.

II. ISLAND MICROGRID ANALYSIS

A. Configuration of Droop Control

The conventional droop control is usually used according to the $P-\omega$ and $Q-V$ law, which can be expressed as

$$\omega_i = \omega^* + k_{pi}(P_{iref} - P_i) \quad (1)$$

$$V_i = V^* + k_{qi}(Q_{iref} - Q_i) \quad (2)$$

where ω_i and V_i are the output angular frequency and voltage amplitude, which are the references for controlling the output voltage; ω^* and V^* give the reference values of the frequency and voltage amplitude. In stand-alone mode, the active power and reactive power references P_{iref} and Q_{iref} are equal to zero. P_i and Q_i indicate the active power and reactive power of the i th unit. The droop factors for the active and reactive power loops, k_{pi} and k_{qi} , are designed in accordance with the maximum power ratings of the inverters.

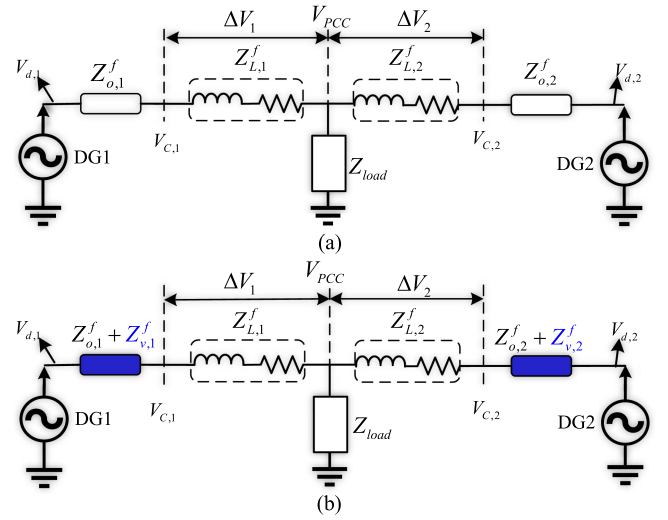


Fig. 1. (a) Effect of feeder mismatch on reactive power sharing. (b) Virtual impedance on reactive power control.

As stated in (1), ω_i is a global variable, suggesting that active power can naturally be shared proportionally. Reactive power sharing, in contrast, becomes more complex given the mismatched feeder impedance and varying control parameters.

B. Reactive Power Sharing Analysis

The voltage drop across the transmission line in [21] can be expressed as

$$\Delta V_i \approx \frac{X_i Q_i + R_i P_i}{V_{C,i}} \quad (3)$$

where X_i and R_i describe the inductance and resistance of the physical feeder. ΔV_i represents the voltage drop and $V_{C,i}$ indicates the filter capacitor voltage.

The effect of feeder and inverter output impedance on reactive power sharing can be illustrated in a simplified microgrid with two inverters, as shown in Fig. 1, where the V_{PCC} represents the voltage point of common coupling. The transfer function under the fundamental frequency and the h th harmonic frequency is denoted by the upper corners f and h , respectively. $Z_{o,i}^f$, $Z_{L,i}^f$, and $Z_{v,i}^f$ indicate the output fundamental impedance, fundamental feeder impedance, and virtual fundamental impedance of i th DG, respectively. $Z_{o,i}^h$, $Z_{L,i}^h$, and $Z_{v,i}^h$ in Fig. 2 denotes the corresponding harmonic components. $V_{d,i}$ is the output of the droop controller.

It is apparent that the resistive component of the feeder, combined with the mismatched inductive impedance, can result in an incorrect share of reactive power. Nevertheless, it is reasonably assumed that the line is inductive, which allows for the restatement of (3) as (4)

$$\Delta V_i \approx \frac{X_{e,i} Q_i}{V_{C,i}} \quad (4)$$

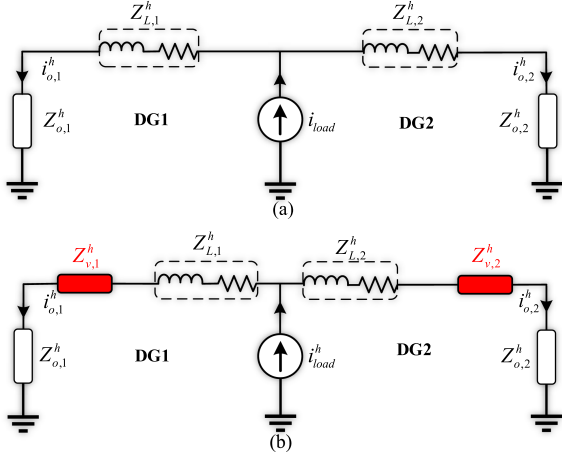


Fig. 2. (a) Effect of feeder mismatch on harmonic current sharing. (b) Virtual impedance on harmonic current control.

where $X_{e,i}$ represents equivalent impedance i -DG. Given that the variation in DG's ΔV_i is small, the reactive power is determined by $X_{e,i}$. It can be derived that when the equivalent impedance ratio inversely corresponds to the maximum output capacity ratio, reactive power can be distributed according to the output capacity. Otherwise, if this condition is not met, where the control parameters and feeder impedances are mismatched, reactive power cannot be appropriately shared.

Fig. 1(b) demonstrates that proper design of the virtual impedance enables modification of the equivalent impedance $X_{e,i}$. This, in turn, allows for the adjustment of the voltage drop among the units, which helps to promote the proportional sharing of reactive power.

C. Harmonic Power-Sharing Analysis

To achieve a proportional harmonic power sharing according to the maximum output power ratio, the requirement below should be considered

$$k_{h1}i_{o,1}^h = k_{h2}i_{o,2}^h = \dots = k_{hi}i_{o,i}^h \quad (5)$$

where k_{hi} is the harmonic sharing coefficient, and represents the inverse of the maximum output harmonic power. $i_{o,i}^h$ denotes the harmonic current of i th-DG. As illustrated in Fig. 2(a), the mismatched harmonic line impedance and inner controller output impedance among different DGs can result in improper sharing of harmonic power, where the nonlinear loads are considered as current sources [16].

To address this issue, the virtual harmonic impedance in Fig. 2(b) is utilized to reshape the overall virtual impedance for specific frequencies as shown in (6), thereby promoting proportional sharing of harmonic power

$$i_{o,1}^h(Z_{o,1}^h + Z_{v,1}^h + Z_{L,1}^h) = i_{o,2}^h(Z_{o,2}^h + Z_{v,2}^h + Z_{L,2}^h). \quad (6)$$

III. FROM COMMUNICATION TO VIRTUAL IMPEDANCE

This section introduces the consensus algorithm-based virtual impedance to facilitate the proportional sharing of reactive and harmonic power.

A. Communication Network Modeling

The communication network involved in the microgrid can be represented by an undirected cyber graph, which shows how the converters share data with their neighbors. For each local converter i th of the microgrid, the communication graph with its neighbors j th can be described as an undirected graph with edges and links via the communication adjacency matrix $A = (a_{ij})_{N \times N}$. The communication weight a_{ij} is set to 1 if the i th and j th units are in regular communication, and 0 otherwise. The degree of vertex ζ_i is given as $d_i = \sum_{j=1}^N a_{ij}$. The corresponding degree matrix is $D = \text{diag}(d_1, \dots, d_N)$. The Laplacian matrix of the communication network, denoted by L , is defined as $L = D - A$.

B. Harmonic Current Extraction and Power Calculation

The second-order generalized integrator is adopted to extract the selected harmonic current $i_{o,i}^h$ [14]. The h th harmonic power of the i th converter is obtained using the rms value $V_{i,\text{rms}}$ of the fundamental voltage, the rms value $i_{o,\text{rms}}^h$ of the harmonic current, and the conjugate signal $i_{o,d}^h$ of the harmonic current, as given by (7). Specifically, $V_{i,\text{rms}}$ is defined as $V_i/\sqrt{2}$

$$H_i = V_{i,\text{rms}}i_{o,i,\text{rms}}^h = \frac{1}{2}V_i\sqrt{(i_{o,i}^h)^2 + (i_{o,id}^h)^2}. \quad (7)$$

C. Communication-Based Virtual Impedance

In Fig. 3, the inverters exchange information related to reactive power ($k_{q1}Q_1^f, \dots, k_{qN}Q_N^f$) and harmonic power ($k_{h1}H_1^h, \dots, k_{hN}H_N^h$) with their adjacent units to achieve a consensus state. The reshaped consensus algorithm-based virtual fundamental impedances are expressed as (8) and (9)

$$Z_{v,i}^f = Z_{0,i}^f + Z_{c,i}^f \quad (8)$$

$$Z_{c,i}^f = \int k_{v,i}^f \left[\sum_{j \in N_i} a_{ij}(k_{qi}Q_i - k_{qj}Q_j) \right] dt. \quad (9)$$

The harmonic impedance can be modulated as (10) and (11)

$$Z_{v,i}^h = Z_{0,i}^h + Z_{c,i}^h \quad (10)$$

$$Z_{c,i}^h = \int k_{v,i}^h \left[\sum_{j \in N_i} a_{ij}(k_{hi}H_i - k_{hj}H_j) \right] dt \quad (11)$$

where N_i represents all adjacent units of i th DG. The fixed virtual inductors $Z_{0,i}^f$ and $Z_{0,i}^h$ are initial virtual impedance values used to improve the impedance's inductive response and, thus, the system's stability. The adaptively adjusted impedance $Z_{c,i}^f$ and $Z_{c,i}^h$ are determined by the neighbor's information and the state of the local unit. The impedance reshaping factors for harmonic and reactive power sharing loops are $k_{v,i}^h$ and $k_{v,i}^f$, respectively.

In practice, the transmitted information exhibits time variation, incorporating time delays. The application of integral controllers is necessary to compensate for harmonic and reactive power-sharing errors. It's noteworthy that the delay in control performance has been detailed in [14]. For brevity, we omitted this aspect in the current presentation.

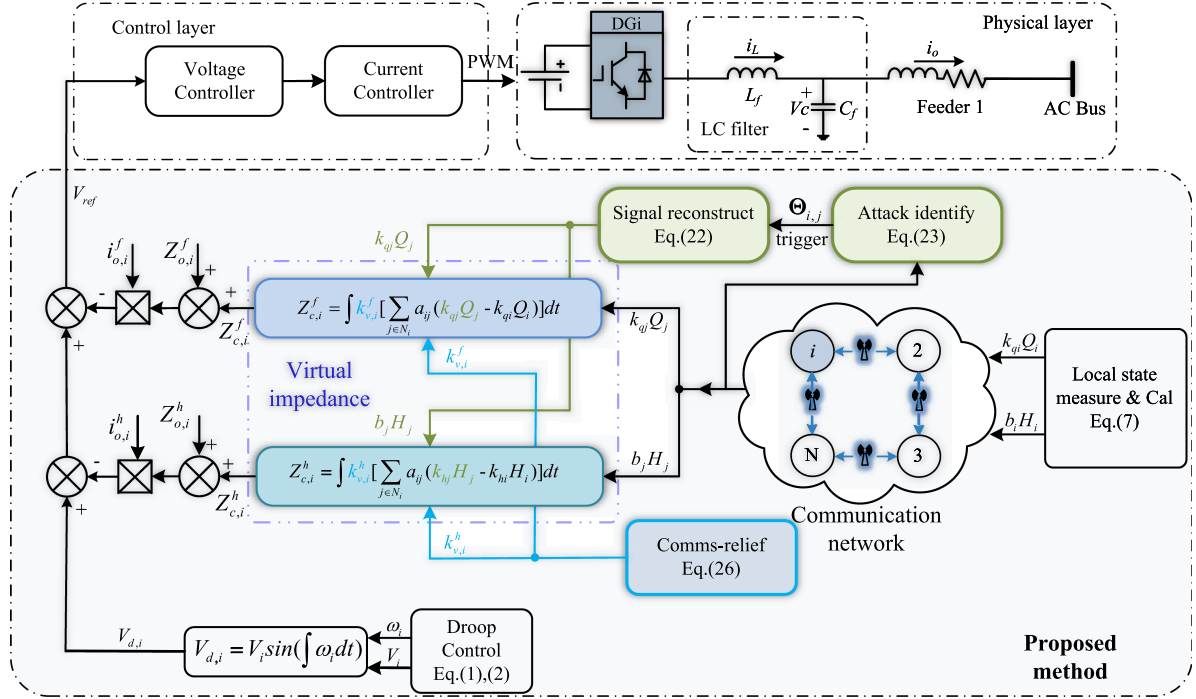


Fig. 3. Comprehensive control block diagram of the proposed method.

With distributed virtual impedance control, the voltage reference for the capacitor voltage modifies as

$$V_C = V_d - Z_v^f i_o^f - Z_v^h i_o^h - Z_o^f i_o^f - Z_o^h i_o^h \quad (12)$$

where the i_o^f represents the fundamental component of the output current. Typically, the converter can be modeled as a voltage source in series with resistance. With the virtual impedance, the filter capacitor voltage V_C is determined by the droop controller output (V_d), virtual impedance (Z_v^f and Z_v^h), converter's output impedance (Z_o^f and Z_o^h), and output current (i_o^f and i_o^h).

IV. IMPROVED RESILIENCE AND COMMUNICATION RELIEF

The proposed virtual impedance effectively enables the proportional sharing of reactive and harmonic power. However, it is susceptible to cyber-attacks and communication disruption. This section first introduces the model for each threat. Then, a resilient controller is designed to immunize the cyber attack and communication disruption by reconstructing the attacked signal. Furthermore, we introduce an auxiliary controller to save communication resources and make it less vulnerable to communication issues by turning off the communication network. It is reasonable since the impact of virtual impedance is equivalent to physical feeder impedance, and if the feeder impedance is properly set, the communication is no longer needed. In this way, without any further communication, the microgrid even maintains the plug-and-play operation.

A. Cyber Attack Analysis

The false data injection attack (FDIA) is a highly concerning type of attack involving injecting false data into the original

signal [24]. The identification of FDIA is detailed in Section IV-D. This attack can be modeled as in the following equation:

$$x_{a,j} = x_j + \eta_j \varepsilon(t) \quad (13)$$

where x_j and $x_{a,j}$ represent the original neighboring and attacked signal, respectively. The binary variable η_j is zero in the normal state and equals one when the false data is inserted into the communication channel. $\varepsilon(t)$ is the malicious element injected into the communication network, which may vary in different links.

For reactive power sharing controller: With the equivalent effect of virtual impedance and feeder impedance, we can intuitively develop an expression for reactive power and fundamental impedance from (4), denoted as $Q_i = H_L^f / (Z_{v,i}^f + Z_{o,i}^f + Z_{L,i}^f)$, where $H_L^f = \Delta V_i V_{C,i}$. Given the existence of FDIA on the communication network, the methods proposed in (8) and (9) can be represented in the following equation:

$$Q_i = \frac{H_L^f}{\int k_{v,i}^f \sum_{j \in N_i} a_{ij} (k_{qi} Q_i - k_{qj} Q_{a,j}) dt + Z_{e,i}^f} \quad (14)$$

where $Z_{e,i}^f$ is the sum of $Z_{0,i}^f$, $Z_{o,i}^f$, and $Z_{L,i}^f$, representing the equivalent value of the fixed fundamental impedance.

The power-sharing error, which is supposed to be 0, is given by the deviation between the reactive power-sharing performance of the i th inverter and its neighbor j th inverter, expressed as $(k_{qi} Q_i - k_{qj} Q_j)$. Here, Q_i^* describes the average output reactive power sharing ratio among the system. In a normal situation ($k_{q1} Q_1 = \dots = k_{qn} Q_n = Q_i^*$). The dynamics of state errors under attacks against communication channels are given as

follows:

$$\dot{Q}_i = \frac{-H_L^f k_{v,i}^f [Lk_{qi}Q_i - B\varepsilon(t)]}{\{\int k_{v,i}^f [Lk_{qi}Q_i - B\varepsilon(t)]dt + Z_{e,i}^f\}^2} \quad (15)$$

where B is the cyber attack incidence matrix.

For harmonic power sharing controller: As shown in Fig. 2, we can also take $H_i = H_L^h / (Z_{v,i}^h + Z_{o,i}^h + Z_{L,i}^h)$, where $H_L^h = \Delta V_i^h V_{C,i}$, representing the inverse of the impedance and the harmonic power. ΔV_i^h is the equivalent harmonic impedance of the i th DG. Combining (10) and (11), the relationship of harmonic power and transmitted information can be shown as follows:

$$H_i = \frac{H_L^h}{\int k_{v,i}^h [\sum_{j \in N_i} a_{ij} (k_{hi}H_i - k_{hj}H_{a,j})dt + Z_{e,i}^h]} \quad (16)$$

where $Z_{e,i}^h$ is the sum of $Z_{0,i}^h$, $Z_{o,i}^h$, and $Z_{L,i}^h$, representing the equivalent value of the fixed harmonic impedance.

The state error of harmonic power sharing is $(k_{hi}H_i - k_{hj}H_j)$. In the normal state, $(k_{h1}H_1 = \dots = k_{hi}H_i = H_i^*)$, where H_i^* represents the average harmonic power-sharing ratio in the system. When the communication channel is subjected to FDIA, the derivative of the harmonic power sharing errors can be written as

$$\dot{H}_i = \frac{-H_L^h k_{v,i}^h [Lk_{hi}H_i - B\varepsilon(t)]}{\{\int k_{v,i}^h [Lk_{hi}H_i - B\varepsilon(t)]dt + Z_{e,i}^h\}^2}. \quad (17)$$

B. Stability Analysis

In this section, the superscript f and h are removed for analysis simplification. To analyze the stability, we consider the Lyapunov function candidate in the following equation:

$$\nu(x) = \frac{1}{2}x^T Lx \quad (18)$$

where x is the state $k_{qi}Q_i$ and $k_{hi}H_i$ of the designed control, in an simplified expression. Combining (15) and (17), the derivative in time of $\nu(x)$ along the trajectories (18) of the two controllers is given by

$$\begin{aligned} \dot{\nu}(x) &= x^T L \dot{x} \\ &= x^T L \frac{-k_i H_L k_{v,i} [Lx - B\varepsilon(t)]}{\{\int k_{v,i} [Lx - B\varepsilon(t)]dt + Z_{e,i}\}^2} \end{aligned} \quad (19)$$

where k_i represents the coefficient k_{qi} and k_{hi} . In (19), without any cyber attacks, that is, $B\varepsilon(t) = 0$ and $\dot{\nu}(x) < 0$ for all $x \neq 0$ at the steady state. This implies that the chosen Lyapunov function is globally asymptotically stable. Hence, $\nu(x)$ ultimately tends to zero, making the state error converge to zero and enabling the reactive and harmonic power to be shared proportionally.

When the grid is subjected to an FDIA with a malicious signal ε , a new state x_p is introduced to clarify the system's dynamics, where $Lx_p = B\varepsilon$. Referring to (19), if $\dot{\nu}(x) < 0$ for any state $x \neq x_p$, the Lyapunov function $\nu(x)$ will ultimately lead the system state to converge to $x = x_p$. In this case, the state error stabilizes at a nonzero value rather than converging

to zero. Consequently, the power-sharing ratio deviates from its predefined value, disrupting the expected power-sharing ratio.

On the other hand, if $Lx_p \neq B\varepsilon$ throughout the feasible domain, the Lyapunov function fails to converge to a new equilibrium point. As a result, both the active power and harmonic power are continuously affected by the FDIA signal, leading to sustained effects on the system's operation.

In summary, the presence of FDIA prevents proportional sharing of active and harmonic power as originally intended, compromising the microgrid's performance and stability.

C. Communication Disruption Analysis

When a communication disruption occurs in the network, the local controller is unable to correctly receive information from its neighbors, which can be denoted as

$$x_{f,j} = \kappa_j x_j \quad (20)$$

where x_j and $x_{f,j}$ represent the original neighboring signal, and the signal arrives at the local controller, respectively. The binary variable $\kappa_j = 1$ represents a regular communication, while $\kappa_j = 0$ denotes the communication disruption between i th and j th DGs. It can be derived that when the communication occurs, the received data from the neighbor is zero, which will contribute to an incorrect command on the local controller. The detailed analysis is similar to Sections IV-A and IV-B, which we have omitted here.

D. Resilience and Communication Relief

This article proposes a resilient enhanced controller as a means to mitigate cyber-attacks and communication disruption. As microgrid communication networks are complex and comprise numerous nodes with varying communication types, it is hypothesized that cyber-attacks and communication disruption targeting a selected inverter unit would not simultaneously disrupt all the communication channels through which it communicates with its neighboring nodes. Moreover, Section I analyzes the communication dependency and identifies it as a challenge in the commutation-based approach. To address this issue, an auxiliary controller is proposed to relieve the communication, before which the virtual impedance has been appropriately modulated to facilitate optimal power-sharing performance.

With the proposed method, the resilient virtual impedance can be rewritten as

$$Z_{c,i} = \int k_{v,i} \sum_{j \in N_i} a_{ij} [(1 - \Theta_{i,j})(x_j - x_i) + \Theta_{i,j} \Delta x_{i,j}^*] dt \quad (21)$$

where $\Delta x_{i,j} = x_j - x_i$, and $\Delta x_{i,j}^* = \min\{|\Delta x_{i,1}|, \dots, |\Delta x_{i,j}|\} \cdot \text{sgn}(\Delta x_{i,j})$. $\text{sgn}(\cdot)$ represents the selected signal's sign. $\text{sgn}(z) = z/|z|$. The variable $\Theta_{i,j}$ is a binary indicator that denotes whether cyber attack and communication disruption have occurred or not

$$\Theta_{i,j} = \begin{cases} 1, & \text{if } |\Delta x_{i,j}| \geq \Upsilon_{i,j} \\ 0, & \text{else.} \end{cases} \quad (22)$$

In this article, we utilize $\Lambda_{i,j}$ to identify the presence of cyber attack and communication disruption. The variable $\Lambda_{i,j}$ represent the difference between the data from the neighboring j th unit and the local state of i th unit, denoted as $\Lambda_{i,j} = a_{ij}(x_j - x_i)$. This identification can be expressed as shown in (22). Considering the general disturbance and measure noise, variable $\Upsilon_{i,j}$ serves as the cyber attack and communication disruption measurements threshold and is defined as $\Upsilon_{i,j} = 0.01x_i$. Based on this definition, if $|\Lambda_{i,j}| \geq \Upsilon_{i,j}$, we conclude that there is a cyber attack or communication disruption and set $\Theta_{i,j} = 1$. Conversely, if $|\Lambda_{i,j}| < \Upsilon_{i,j}$, we determine that there is regular communication.

When confronted with FDIA, the neighbor's information is manipulated, introducing deliberate deviation. Differently, during instances of communication disruption, the neighbor's data is intentionally set to zero. This different character enables the system to distinguish between a potential cyberattack and a mere communication breakdown.

If a cyber attack or communication disruption occurs between the j th and i th DG units, a binary signal $\Theta_{i,j}$ is sent to the reconstructing controller. Thereby, the corrupted communication link that is attacked is replaced by a healthy signal reconstructed using $\Delta x_{i,j}^*$. This procedure benefits that the proposed communication-based strategy is resilience enhanced.

In addition, the signal reconstruction benefits do not damage the network convergence rate, which can be analyzed as follows.

Based on the reactive power and harmonic power difference terms in (9) and (11), with the adopted communication graph, the Laplacian disagreement function of the graph is defined as the difference between neighboring DGs

$$\Phi_{G(x)} = x^T L x = \frac{1}{2} \sum_{j \in N_i} a_{ij} (x_j - x_i)^2 \quad (23)$$

where x_i represents the variable associated with reactive power $k_{qi}Q_i$ and harmonic power $k_{hi}H_i$.

The Laplacian matrix of the graph satisfies the following property [25]:

$$\lambda_2(L) = \min_{x \neq 0, 1^T x = 0} \frac{x^T L x}{\|x\|^2} \quad (24)$$

where $\lambda_2(L)$ represents the second smallest eigenvalues of the Laplacian matrix L , which denotes the algebraic connectivity of the undirected graph. Based on the Fiedler eigenvalue, a larger $\lambda_2(L)$ means stronger connectivity and a faster convergence speed.

Fig. 4 shows different communication connections of the DGs. Supposing the system is subject to cyber-attack, and the signal on the communication link 2-1 is corrupted, as shown in Fig. 4(a). As shown in Fig. 4(b), from the authors in [22] and [23], it is suggested to block the corrupted link, which may reduce algebraic connectivity. Remarkably, the proposed method shown in Fig. 4(c) can benefit from greater algebraic connectivity by reconstructing the corrupted method compared to [22], [23]. This can be proved from the Laplace matrix $\lambda_2(L_b) < \lambda_2(L_c)$, where L_b represents the Laplacian matrix of Fig. 4(b), and L_c is the Laplacian matrix of Fig. 4(c).

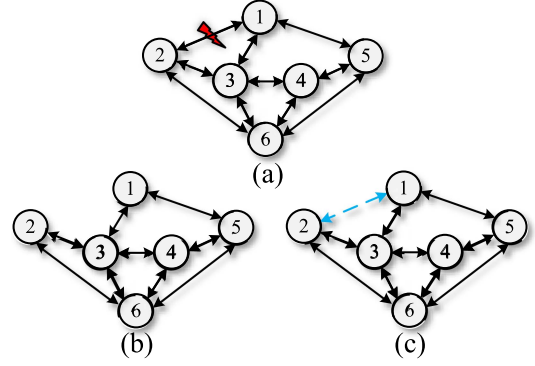


Fig. 4. (a) Original attacked graph. (b) Proposal in [22] and [23]. (c) Proposed method.

Herein, the numerical verification of the convergence rate is presented. The eigenvalues of the Laplacian matrices, $\lambda_2(L_b)$ and $\lambda_2(L_c)$, associated with Fig. 4(b) and (c), respectively, are calculated, as shown in Fig. 5.

Based on the adjacency graphs in Fig. 4(b) and (c), the corresponding adjacency tables are derived. According to Section III-A, the adjacency matrix A and the degree matrix D are obtained. Subsequently, the Laplacian matrix is calculated as $L = D - A$. Therefore, the eigenvalues of the Laplacian matrix are found to be $\lambda_2(L_b) = 1.6072 < \lambda_2(L_c) = 2.2679$. Based on the Fiedler eigenvalue, the method depicted in Fig. 4(c) demonstrates a faster convergence rate compared to the method in Fig. 4(b).

Moreover, the proposed method can reduce the communication dependency by utilizing an auxiliary controller to deactivate communication, which can be expressed as follows:

$$k_{v,i} = \begin{cases} 0, & \text{if } \Theta_{i,j} \cup \Theta_{i,2} \cdots \cup \Theta_{i,N} = 0 \\ k_{v,i}, & \text{else.} \end{cases} \quad (25)$$

Assuming that the inverter system has been constructed by using the proposed method, it is expected that the sharing of harmonic and reactive power among all units will be proportional, thus satisfying the “steady state” requirements for all nodes $i \in N_i$ as denoted by $|\Lambda_{i,j}| < \Upsilon_{i,j}$. In such a scenario, the auxiliary controller is triggered, assigning a value of 0 to reshape factor, represented as $k_{v,i} = 0$. Consequently, the microgrid becomes independent of the communication network. In other words, the communication relief method implementation involves a two-step process. Initially, the DGs adjusts the virtual impedance in response to disparities with their neighbors. Subsequently, the consistent maintenance of power-sharing is achieved by upholding a constant virtual impedance value. This eliminates the need for continual communication, even in case of load change and plug-and-play operation.

V. EXPERIMENT RESULTS

The efficacy of the proposed adaptive control strategy has been verified through experiments conducted on a distributed ac microgrid consisting of three parallel-connected inverters. The experimental setup, illustrated in Fig. 6, shows that each inverter

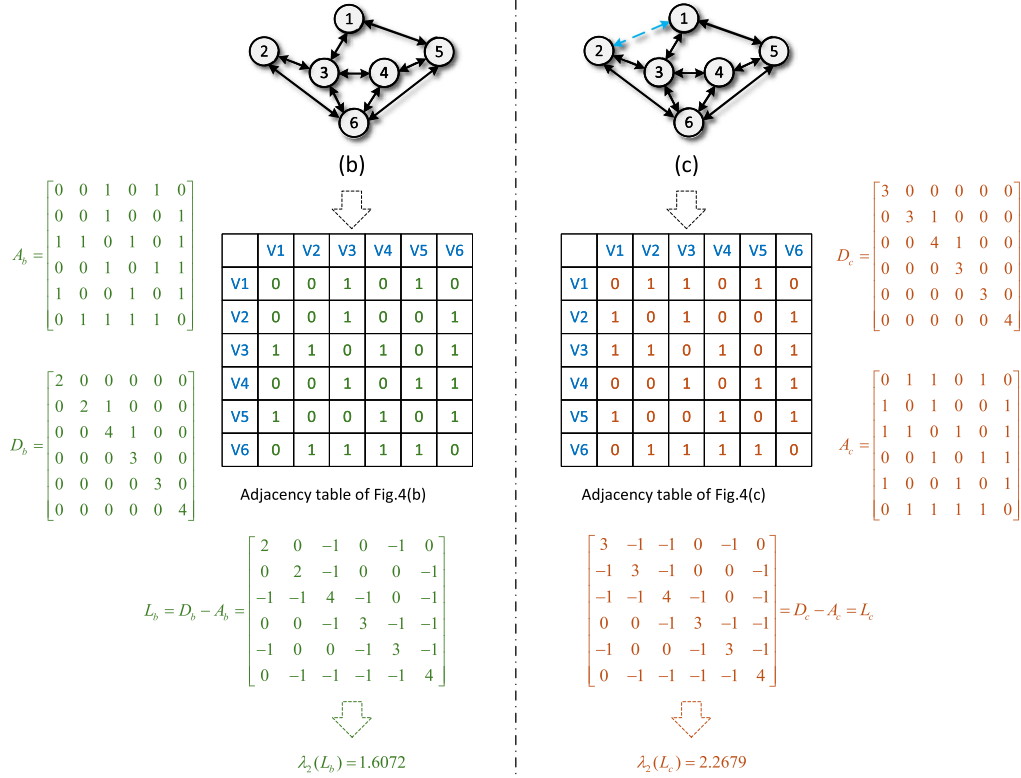


Fig. 5. Numerical verification of the convergence rate in Fig. 4(b) and (c).

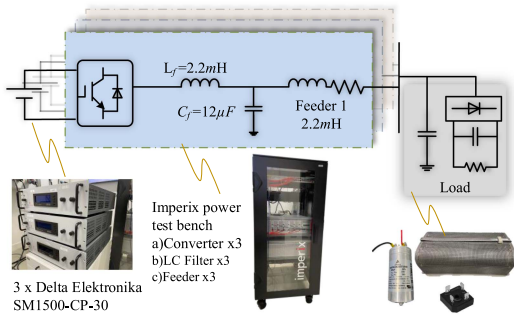


Fig. 6. Experiment setup.

TABLE II
PARAMETERS OF THE MICROGRID IN EXPERIMENT

Symbol	Interpretation	Value
U_{dc}	DC-link voltage	150 V
Z_L	Line impedance	2.2 mH
L_f	Inductor of LC filter	2.2 mH
C_f	Capacitor of LC filter	12 μ F
f_s	Switch frequency	20 kHz
k_{p1}, k_{q1}	droop coefficient of DG1	1/1000
k_{p2}, k_{q2}	droop coefficient of DG2	1/2000
k_{p3}, k_{q3}	droop coefficient of DG3	1/3000
$k_{v,i}^f$	fundamental impedance reshape factor	0.001
$k_{v,i}^h$	harmonic impedance reshape factor	0.001
ω^*	Nominal angular frequency	314 rad/s
V^*	Nominal voltage amplitude	110 V

communicates with the other two units for secondary control. The parameters are provided in Table II.

In this article, the third harmonic is utilized to validate the performance of the harmonic control. The harmonics and reactive power output of the inverters adhere to the maximum power ratio, which is assumed to be 1:2:3. In practice, this ratio can be adjusted to any given value. To verify the effectiveness of the proposed method, experiments are conducted under several scenarios. The test procedures for the main cases are illustrated in Fig. 7.

Case A: Comparing the performance of power-sharing mechanisms before and after implementing the proposed

communication-based virtual impedance; evaluating the system's ability to immunize the effects of communication delays and disruption and load variations.

Case B: Exploring the potential effects of cyber attacks on power-sharing and assessing how the proposed defense mechanism can mitigate these effects.

Case C: A comparative study with two recent studies is conducted to demonstrate the benefits of this article's power-sharing performance and plug-and-play capability in no-communication situations.

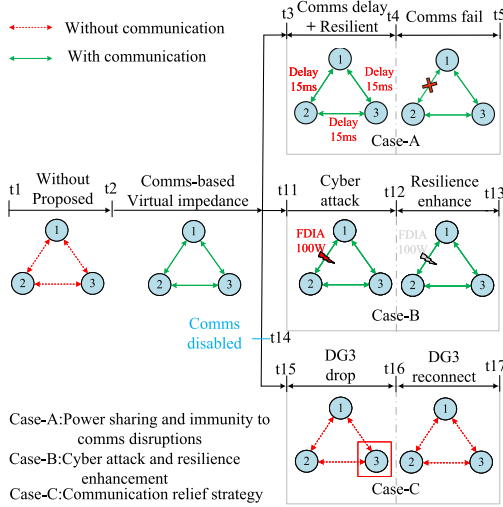


Fig. 7. Experimental procedure.

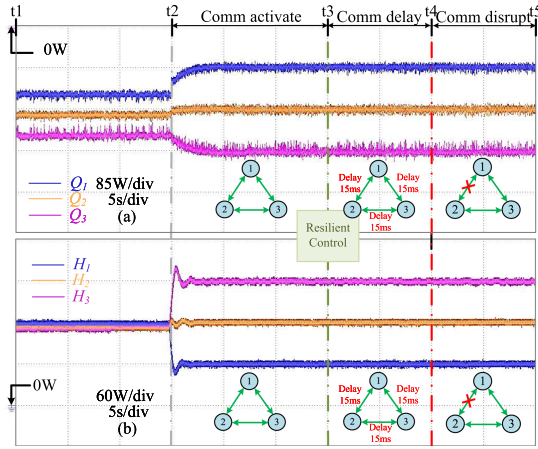


Fig. 8. Power sharing performance of the proposed controller. (a) Reactive power. (b) Third harmonic power.

It should be noted that connecting all units to the microgrid may require a significant amount of time, during which a cyber attack could occur through communication channels. Therefore, we address both mitigating cyber attacks and reducing communication burdens. Subsequently, proposing disabling communication when the virtual impedance is well-tuned. This can alleviate communication dependency and reduce the risk of further cyber attacks and disruptions.

A. Power Sharing Under Communication Disruptions

Initially, as shown in Fig. 8(a) and (b) during the $t1$ – $t2$ stage, reactive and harmonic power sharing is inaccurate due to mismatched feeder impedance and control parameters. It should be noted that the different droop coefficient only affects the fundamental impedance, as there is no droop control loop for harmonic power. In contrast, the other control parameters and feeder impedance remain the same, resulting in the sharing of harmonic power in a 1:1:1 ratio.

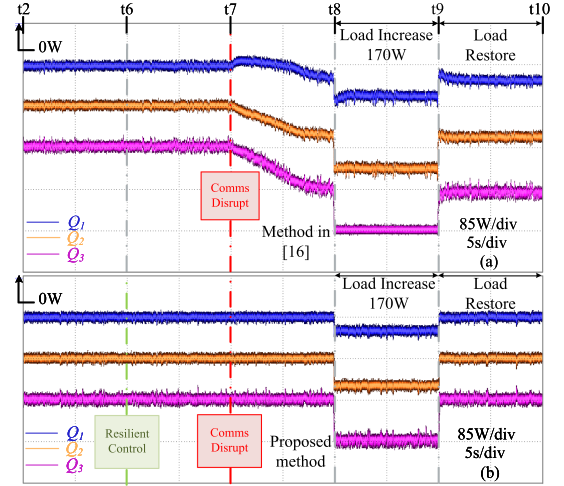


Fig. 9. Comparison of reactive power performance with different strategies under communication disruption. (a) Distributed virtual impedance control in [16]. (b) Proposed resilient method.

Subsequently, with the activation of the virtual impedance at $t2$, proportional sharing of reactive and harmonic power is achievable, regardless of the initial condition. Remarkably, at $t3$, the resilient control is enabled, and the power-sharing performance remains unaffected, despite a communication delay of 15 ms and communication loss imposed on the communication link from DG2 to DG1 at $t3$ and $t4$, respectively.

A comparison study with [16] under the communication disruption scenario is illustrated in Fig. 9. In Fig. 9(a), the influence of a communication interruption on the output reactive power is visible when applying the virtual impedance proposed in [16]. Specifically, at $t7$, the communication link 3-1 experiences an interruption, resulting in a drop of the reactive power, which subsequently affects the load switch operation. This drop occurs because the transmitted information is interrupted by the failure, leading to unreasonable virtual impedance adjustment and a continued decrease in capacitor voltage. The nadir of reactive power is limited by the virtual impedance limiter. This suggests that communication failure results in decreased reactive power, which cannot meet the load demand. By contrast, Fig. 9(b) shows that the proposed method exhibits improved resilience to communication disruption. Resilient control is activated at $t6$ in this case, ensuring that reactive power performance stays unaffected by the communication disruption at $t7$. Moreover, during load fluctuations at $t8$ and $t9$, where the load increases by 170 W and then recovers, the power-sharing ratio remains consistently maintained. This indicates that the suggested resilient control will not degrade the operation of the microgrid during the load change.

B. Test of Resilience

Fig. 10(a) and (b) illustrates the effects of cyber attacks on the microgrid secondary control and the effectiveness of the suggested resilient control for mitigating such attacks, respectively. During the $t2$ – $t11$ stages, the communication-based

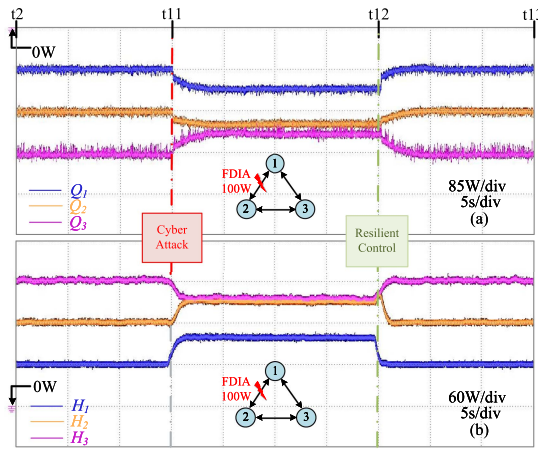


Fig. 10. Effect of cyber attack and performance of the resilient controller. (a) Reactive power. (b) Third harmonic power.

virtual impedance is employed. This allows an appropriate distribution of reactive power and harmonic power, and there is no cyber attack on the communication network during this period. Then, the communication channel from DG2 to DG1 is attacked by an FDIA with $\varepsilon(t) = 100$ W upon the reactive power and harmonic power controllers at t_{11} . Consequently, the power-sharing ratio moves away from the optimal value. At t_{12} , the suggested resilient framework is activated, removing the distorted data and reconstructing the attacked signal, thereby restoring the power-sharing ratio to 1:2:3. The findings exhibit the proposed approach's resilience to cyber-attacks.

C. Test of Communication Relief

As stated in Section I, the proposed methodology can potentially reduce the communication dependency by deactivating the communication network when all participating inverters are connected and properly adjusted. At this stage, the reactive and harmonic power can be shared accurately since the virtual impedance is already well-tuned. Fig. 11 demonstrates that the proposed control method featuring a communication relief strategy outperforms several recent studies.

Fig. 11(a) and (b) showcases the reactive power performance of the distributed method in [15], [16], [21], [22], and [23] in no communication scenario, respectively. Meanwhile, Fig. 11(c) and (d) depicts the reactive power and fundamental current employing our proposed method under the same circumstances.

Notably, the communication network is deactivated at t_{14} , before which distributed control loops are employed to facilitate power-sharing. During the subsequent period from t_{14} to t_{15} , as the communication is disabled, the distributed virtual impedance in [15], [16], and [21] promptly loses its effectiveness, resulting in an improper in the power-sharing ratio, which deviates from the expected 1:2:3 distribution. Furthermore, in this case, the plug-and-play test becomes unreliable, as the reactive power cannot be proportionally shared within the operational DGs.

Differently, at t_{15} , as depicted in Fig. 11(b)–(d), when DG3 is unplugged, the method presented in [22] and [23] fails to

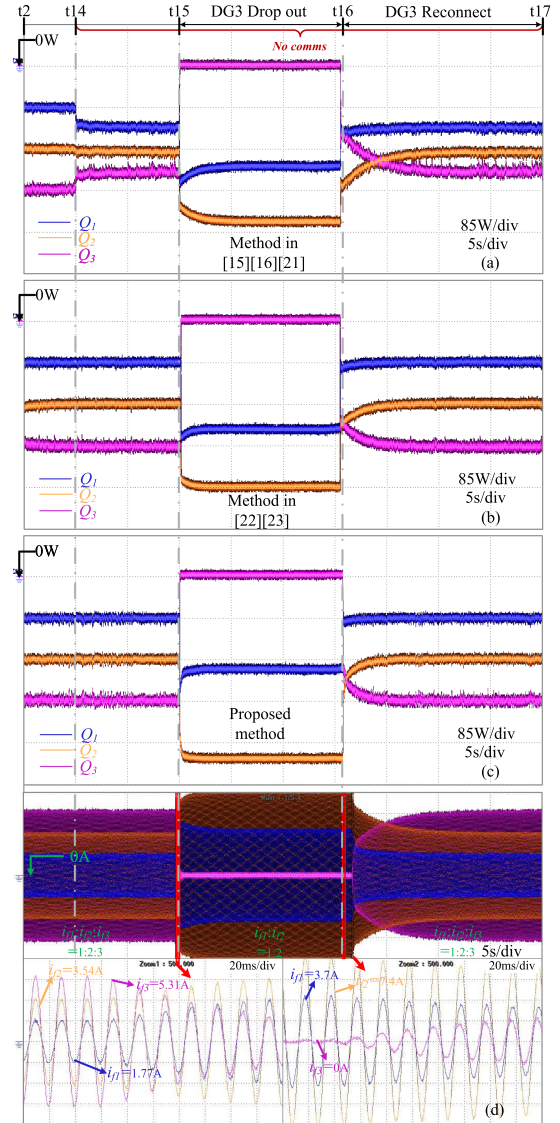


Fig. 11. Comparison of plug-and-play operation with different strategies in the no-communication scenario. (a) Distributed virtual impedance [15], [16], [21]. (b) Voltage compensation method in [22] and [23]. (c) Reactive power of the proposed method. (d) Fundamental current of the proposed scheme.

ensure that operational DG1 and DG2 share reactive power in an accurate 1:2 ratio. However, with this method, the microgrid can promise the desired power-sharing ratio when the DG3 is reconnected. This underscores the reliance of the two aforementioned methods on continuous communication networks for seamless plug-and-play operation.

In contrast, the proposed method, from t_{14} to t_{17} , maintains a stable expected power-sharing ratio among the participating inverters without the need for continuous communication. This is achieved through an appropriately adjusted and pre-fixed virtual impedance. Consequently, Fig. 11 demonstrates that the proposed control method imposes significantly lower communication demands than the abovementioned two existing methods.

VI. CONCLUSION

Consensus algorithm-based virtual impedance helps the microgrids achieve reactive and harmonic power sharing. It, however, exposes the system to cyber-attacks and other communication failures. The proposed signal reconstruction approach only needs communication shortly after each new DG's cut-in. By decreasing the weight of the communicated signal that deviates more from the average, the impact of communication failure is largely reduced. Moreover, a healthy signal is reconstructed to maintain a fast convergence speed. Furthermore, the memory effect of the proposed signal reconstruction approach allows the communication to be switched-OFF once the virtual impedance is established, thereby further reducing the system's vulnerability. The Lyapunov stability analysis shows that the power-sharing of the system will still converge to the same point even under communication failure, which cannot be achieved without the proposed approach. The experiment results verify the effectiveness of the proposed approach.

The proposed method reconstructs the corrupted signal from the healthy channel. However, in the case of more malicious attacks where all channels are compromised, leaving no healthy signals, the proposed method may lose its effectiveness. This limitation will be investigated in future work.

REFERENCES

- [1] B. Chen, J. Wang, X. Lu, C. Chen, and S. Zhao, "Networked microgrids for grid resilience, robustness, and efficiency: A review," *IEEE Trans. Smart Grid*, vol. 12, no. 1, pp. 18–32, Jan. 2021.
- [2] X. Meng, J. Liu, and Z. Liu, "A generalized droop control for grid-supporting inverter based on comparison between traditional droop control and virtual synchronous generator control," *IEEE Trans. Power Electron.*, vol. 34, no. 6, pp. 5416–5438, Jun. 2019.
- [3] Z. Wang et al., "Active power oscillation suppression based on decentralized transient damping control for parallel virtual synchronous generators," *IEEE Trans. Smart Grid*, vol. 14, no. 4, pp. 2582–2592, Jul. 2023.
- [4] H. Mahmood, D. Michaelson, and J. Jiang, "Accurate reactive power sharing in an islanded microgrid using adaptive virtual impedances," *IEEE Trans. Power Electron.*, vol. 30, no. 3, pp. 1605–1617, Mar. 2015.
- [5] P. Sreekumar and V. Khadkikar, "A new virtual harmonic impedance scheme for harmonic power sharing in an islanded microgrid," *IEEE Trans. Power Del.*, vol. 31, no. 3, pp. 936–945, Jun. 2016.
- [6] Y. Zhu, F. Zhuo, F. Wang, B. Liu, and Y. Zhao, "A wireless load sharing strategy for islanded microgrid based on feeder current sensing," *IEEE Trans. Power Electron.*, vol. 30, no. 12, pp. 6706–6719, Dec. 2015.
- [7] Z. Li, K. W. Chan, J. Hu, and J. M. Guerrero, "Adaptive droop control using adaptive virtual impedance for microgrids with variable PV outputs and load demands," *IEEE Trans. Ind. Electron.*, vol. 68, no. 10, pp. 9630–9640, Oct. 2021.
- [8] J. Chen, L. Wang, L. Diao, H. Du, and Z. Liu, "Distributed auxiliary inverter of urban rail train—load sharing control strategy under complicated operation condition," *IEEE Trans. Power Electron.*, vol. 31, no. 3, pp. 2518–2529, Mar. 2016.
- [9] T. Vandoorn, B. Meersman, J. De Kooning, and L. Vandevelde, "Controllable harmonic current sharing in islanded microgrids: DG units with programmable resistive behavior toward harmonics," *IEEE Trans. Power Del.*, vol. 27, no. 2, pp. 831–841, Apr. 2012.
- [10] J. He, Y. W. Li, and M. S. Munir, "A flexible harmonic control approach through voltage-controlled DG-grid interfacing converters," *IEEE Trans. Ind. Electron.*, vol. 59, no. 1, pp. 444–455, Jan. 2012.
- [11] F. Deng, W. Yao, X. Zhang, Y. Tang, and P. Mattavelli, "Review of impedance-reshaping-based power sharing strategies in islanded ac microgrids," *IEEE Trans. Smart Grid*, vol. 14, no. 3, pp. 1692–1707, May 2023.
- [12] E. Hammad, A. Farraj, and D. Kundur, "On cyber-physical coupling and distributed control in smart grids," *IEEE Trans. Ind. Informat.*, vol. 15, no. 8, pp. 4418–4429, Aug. 2019.
- [13] M.-D. Pham and H.-H. Lee, "Effective coordinated virtual impedance control for accurate power sharing in islanded microgrid," *IEEE Trans. Ind. Electron.*, vol. 68, no. 3, pp. 2279–2288, Mar. 2021.
- [14] T. V. Hoang and H.-H. Lee, "Virtual impedance control scheme to compensate for voltage harmonics with accurate harmonic power sharing in islanded microgrids," *IEEE Trans. Emerg. Sel. Topics Power Electron.*, vol. 9, no. 2, pp. 1682–1695, Apr. 2021.
- [15] Z. Wang et al., "Impedance-based adaptively reshaping method for enhancing nonlinear load sharing and voltage quality in islanded microgrids with virtual synchronous generator," *IEEE Trans. Smart Grid*, vol. 13, no. 4, pp. 2568–2578, Jul. 2022.
- [16] Z. Wang et al., "Adaptive harmonic impedance reshaping control strategy based on a consensus algorithm for harmonic sharing and power quality improvement in microgrids with complex feeder networks," *IEEE Trans. Smart Grid*, vol. 13, no. 1, pp. 47–57, Jan. 2022.
- [17] T. Zhao, Z. Li, and Z. Ding, "Consensus-based distributed optimal energy management with less communication in a microgrid," *IEEE Trans. Ind. Informat.*, vol. 15, no. 6, pp. 3356–3367, Jun. 2019.
- [18] T. Yang, S. Sun, and G.-P. Liu, "Distributed discrete-time secondary cooperative control for AC microgrids with communication delays," *IEEE Trans. Ind. Electron.*, vol. 70, no. 6, pp. 5949–5959, Jun. 2023.
- [19] L. Ding, Q.-L. Han, X. Ge, and X.-M. Zhang, "An overview of recent advances in event-triggered consensus of multiagent systems," *IEEE Trans. Cybern.*, vol. 48, no. 4, pp. 1110–1123, Apr. 2018.
- [20] L. Ding, Q.-L. Han, and X.-M. Zhang, "Distributed secondary control for active power sharing and frequency regulation in islanded microgrids using an event-triggered communication mechanism," *IEEE Trans. Ind. Informat.*, vol. 15, no. 7, pp. 3910–3922, Jul. 2019.
- [21] J. Lu, M. Savaghebi, B. Zhang, X. Hou, Y. Sun, and J. M. Guerrero, "Distributed dynamic event-triggered control for accurate active and harmonic power sharing in modular on-line ups systems," *IEEE Trans. Ind. Electron.*, vol. 69, no. 12, pp. 13045–13055, Dec. 2022.
- [22] J. Xiao, L. Wang, Z. Qin, and P. Bauer, "A resilience enhanced secondary control for AC microgrids," *IEEE Trans. Smart Grid*, vol. 15, no. 1, pp. 810–820, Jan. 2024.
- [23] W. Yao, Y. Wang, Y. Xu, and C. Deng, "Cyber-resilient control of an islanded microgrid under latency attacks and random DoS attacks," *IEEE Trans. Ind. Informat.*, vol. 19, no. 4, pp. 5858–5869, Apr. 2023.
- [24] Y. Liu, Y. Li, Y. Wang, X. Zhang, H. B. Gooi, and H. Xin, "Robust and resilient distributed optimal frequency control for microgrids against cyber attacks," *IEEE Trans. Ind. Informat.*, vol. 18, no. 1, pp. 375–386, Jan. 2022.
- [25] R. Olfati-Saber and R. Murray, "Consensus problems in networks of agents with switching topology and time-delays," *IEEE Trans. Autom. Control*, vol. 49, no. 9, pp. 1520–1533, Sep. 2004.